



**HAL**  
open science

## 3D slab breakoff in laboratory experiments

Carlos Fernández-García, Benjamin Guillaume, Jean-Pierre Brun

► **To cite this version:**

Carlos Fernández-García, Benjamin Guillaume, Jean-Pierre Brun. 3D slab breakoff in laboratory experiments. *Tectonophysics*, 2019, 773, pp.228223. 10.1016/j.tecto.2019.228223 . insu-02369986

**HAL Id: insu-02369986**

**<https://insu.hal.science/insu-02369986>**

Submitted on 20 Nov 2019

**HAL** is a multi-disciplinary open access archive for the deposit and dissemination of scientific research documents, whether they are published or not. The documents may come from teaching and research institutions in France or abroad, or from public or private research centers.

L'archive ouverte pluridisciplinaire **HAL**, est destinée au dépôt et à la diffusion de documents scientifiques de niveau recherche, publiés ou non, émanant des établissements d'enseignement et de recherche français ou étrangers, des laboratoires publics ou privés.



## 3D slab breakoff in laboratory experiments

Carlos Fernández-García\*, Benjamin Guillaume, Jean-Pierre Brun

Univ Rennes, CNRS, Géosciences Rennes, UMR 6118, Rennes, France



### ARTICLE INFO

#### Keywords:

Analogue modelling  
Continental subduction  
Slab breakoff  
Passive margin  
Topography

### ABSTRACT

We study slab breakoff of subducting plates with variable orientations of passive margins (ocean-continent transition: OCT) using three-dimensional laboratory experiments. Our results show that the initial obliquity of the OCT with the trench determines the depth and timing of slab breakoff. The reference model involves a straight OCT parallel to the trench. Slab breakoff first starts in the central section of the subduction zone at a depth equivalent to  $\sim 250$  km and then propagates rapidly towards the edges of the subduction zone where it develops at slightly higher depths ( $\sim 280$  km). In the models where passive margin arrives first at the edges of the subduction zone, slab breakoff starts at that location and propagates laterally towards the center of the subduction zone. It results in higher slab breakoff depths at the edges of the subduction zone than at the center (maximum difference of 170 km). In models where the passive margin arrives first in the center of the subduction zone, slab-breakoff starts at that location and propagates towards the edges of the subduction zone over a period that can be as large as 31 Ma and with a large range of depths (maximum difference of 170 km). The rate of lateral propagation of slab breakoff decreases with the increasing initial obliquity of the OCT with the trench. The model with the maximum obliquity shows a correlation between the surface topography and the slab breakoff at depth. The plate surface is uplifted after the oceanic and continental slab segments are mechanically decoupled, and in the final stage of the experiment, when the slab is educted, subsidence develops as the isostatic and dynamic support diminish.

### 1. Introduction

Slab pull is generally considered as the main driving force for plate motions (Forsyth and Uyeda, 1975; Royden, 1993), and is caused by the negative buoyancy of a subducting oceanic lithosphere. The progressive consumption of oceanic lithosphere at subduction zones can lead to the closure of oceans and to the arrival at the trench of continental lithosphere (e.g., Rosenbaum et al., 2002). The positive buoyancy force that results from the continental lithosphere subduction acts as a force opposing to the oceanic lithosphere slab pull, leading to slab stretching, necking and ultimately to breakoff (Davies and von Blanckenburg, 1995; Ton and Wortel, 1997). In nature, the breakoff of the subducted lithosphere can be indirectly identified by looking at surface changes resulting from perturbations of slab pull and mantle dynamics at depth. In particular, it has been proposed that uplift, sudden changes in deformational regime, changes in magmatic products or fast exhumation of High Pressure rocks may result from slab breakoff at depth. For example, Hippolyte et al. (1994) proposed slab breakoff as a mechanism to explain the uplifted Apenninic belt and the subsequent changes in the stress field from compression before the Middle Pleistocene to extension perpendicular to orogenic axis afterwards. Westaway (1993) indicated

that the high uplift rates observed in the south-western Italy (compared to the eastern coast) could be related to the breakoff beneath the Calabria region in the Middle Pleistocene. Davies and von Blanckenburg (1995) proposed for the first-time slab breakoff in the Alps to explain the evolution of the Tertiary magmatism, uplift, and exhumation of subducted continental rocks. Brun and Faccenna (2008) proposed for the Calabrian-Apennines and Aegean subduction zones that subduction of a buoyant continental lithosphere into the mantle can trigger slab rollback followed by slab breakoff, creating space for the exhumation of HP rocks. Therefore, slab breakoff has an imprint on the geological record and the surface topography that can be recognized and tracked in the field.

An important effort has been made in the last years to better understand the dynamics of slab breakoff. In particular, numerical modeling studies have shown that breakoff depths are significantly influenced by the age and the implemented rheology in the subducting plate. As a result, the slab breakoff in these models develops over a broad range of depths (80–510 km) and requires between 1 and 50 My for the slab breakoff after the arrival of continental lithosphere at the trench (Fig. 1 and Table 1) (Gerya et al., 2004; Baumann et al., 2010; van Hunen and Allen, 2011; Duretz et al., 2014; Schellart, 2017; Magni

\* Corresponding author.

E-mail address: [Carlos.fernandez-garcia@univ-rennes1.fr](mailto:Carlos.fernandez-garcia@univ-rennes1.fr) (C. Fernández-García).

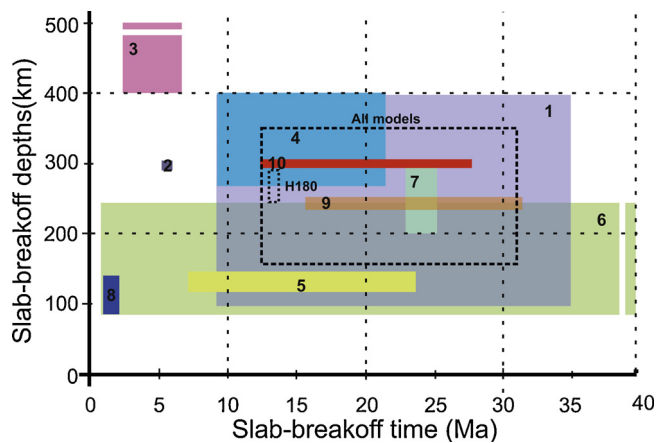


**Fig. 1.** Compilation of slab breakoff depths and timing after the onset of the continental subduction from previous modeling studies (see Table 1 for references). Minimum and maximum values for the models presented in this study are represented by the dashed rectangle. The reference model (H-180) is indicated with a dotted frame.

**Table 1**

Slab breakoff depths and timings obtained in previous analogue and numerical models.

Slab breakoff depths <sup>a</sup> (km)	Slab breakoff time <sup>b</sup> (Myr)	References	Key in Fig. 1
100-400	9-35	Gerya et al. (2004)	1
300	7	Regard et al. (2008)	2
405-510	2.5-6.7	Baumann et al. (2010)	3
280-400	9-21	Van Hunen and Allen (2011)	4
120-145	7-23	Duretz et al. (2014)	5
80-240	2-50	Freeburn et al. (2017)	6
200-300	23-35	Magni et al. (2017)	7
95-140	1.5-2.5	Schellart (2017)	8
240-260	16-32	Broerse et al. (2019)	9
290-310	12.5-27	Hertgen (2018)	10

<sup>a</sup> Range of depths at which the full break-off occurs.

<sup>b</sup> Time to the full breakoff since the arrival at the trench of the continental plate.

et al., 2017; Freeburn et al., 2017; Hertgen, 2018).

Various attempts have also been made to study slab breakoff development using analogue models (Fig. 1). Regard et al. (2008), for instance, investigated slab breakoff by using lithospheric models made of a two-layer system (PDMS silicone mixed with iron fillers and sand) and by imposing horizontal convergence with a piston. While these models show that slab break-off may impact the successive subduction polarities, they have some limitations. In particular, the slab can interact with the bottom of the experimental tank before the breakoff while this interface that corresponds to a 1600–1700 km depth discontinuity has no equivalent on Earth. Boutelier and Cruden (2017) also simulated slab breakoff using a thermomechanical setup consisting of a fixed overriding plate and a subducting plate made of thixotropic dispersions of solid hydrocarbons and powders in oil that are sensitive to the temperature and to strain rates. They concluded that the slower the convergence rate is, the sooner the slab breaks off. However, these models also have some limitations, such as the use of a low-viscosity fluid (water) to model the sub-lithospheric mantle that results in an overestimated subduction velocity for the detached slab segment (~10 m/yr in their Experiment 4). Recently, Broerse et al. (2019) showed that a proper mix of PDMS, iron filler, silicone oil, and plasticine could produce a material with a power-law rheology, capable of localizing deformation at stress levels typically recorded in the laboratory. While encouraging, the results presented in their study are

only preliminary and would require further testing.

All these studies have provided essential insights into the dynamics of slab breakoff and its consequences at the surface, but they also lack essential ingredients to fully comprehend slab breakoff in natural systems. In particular, most of the numerical models are 2-D and as such do not incorporate critical 3D effects (toroidal mantle flow, lateral propagation of slab breakoff). 3D experiments (analogue and numerical models) integrate such effects but generally do not consider the lateral variability of the subducting lithosphere that may exist in natural systems. In particular, they all treat the ocean-continent transition (OCT) as a straight boundary, parallel to the trench, while a broader range of geometries and orientations for the OCT may exist in nature (e.g., Banda Arc). Spakman and Hall (2010) suggested that the present-day morphology of the Banda Arc is the consequence of the Banda oceanic slab affected by rollback since 15 Ma. According to their reconstruction, at that time, the transition from oceanic to continental lithosphere in the subducting plate was not parallel to the trench, and continental subduction started in the northern part of the Banda arc.

In this study, we present the first series of 3D analogue models with different OCT geometries. For this, we systematically change the angle between the OCT direction in the subducting plate and the trench direction. We analyze the effects of the OCT geometry on the timing and the depth of the subsequent slab breakoff. Further, we analyze the rate of slab breakoff lateral propagation and its topographic signature. Finally, we discuss the implications of our results for natural convergence zones.

## 2. Model set-up

### 2.1. Materials and scaling

Our subduction set-up consists of two layers made of visco-elastic PDMS silicone representing the subducting lithosphere and glucose syrup simulating the sub-lithospheric mantle (Table 2), as implemented in previous studies (e.g., Funicello et al., 2003; Bellahsen et al., 2005; Martinod et al., 2005; Schellart, 2005; Guillaume et al., 2010; Husson et al., 2012). In our models, the thermal convection is neglected. The mantle flows only under stresses resulting from the slab sinking. The subducting plate is free to move, responding self-consistently to the subduction dynamics and sinks into the mantle under its own weight. The overriding plate is not simulated in our setup. We therefore assume that it would passively follow the motion of the trench, without modifying the general behavior of the subduction system.

In our setup (Fig. 2), we assume no viscosity jump at the transition between the upper and the lower mantle. We simulate cases for which the subducting lithosphere penetrates directly into the lower mantle, as documented in several subduction zones (Goes et al., 2017). We stop the experiments before the slab reaches the bottom of the box, which here does not represent any natural discontinuity.

Our models reproduce the arrival of a continental lithosphere at the trench following the subduction of an oceanic lithosphere. To achieve this, a 20 cm wide (1500 km in nature) plate of PDMS silicone mixed with sand (continental lithosphere) is attached to the trailing edge of a silicone plate made of a mixture of PDMS and iron powder (oceanic lithosphere) (Fig. 2 and Table 2). The average density contrast of the two attached plates with the underlying glucose syrup is 280 kg/m<sup>3</sup> and

**Table 2**

Material properties and scaling of parameters in nature and in the laboratory.

Models	$\alpha$ (°)	L (cm)	l-1 (cm)	l-2 (cm)	H (cm)	S (cm)
H-110	110	20	18	11	1	0.6
H-150	150	20	18	15.5	1	0.6
H-180 (reference)	180	20	18	18	1	0.6
H-210	210	20	15.5	18	1	0.6
H-250	250	20	11	18	1	0.6

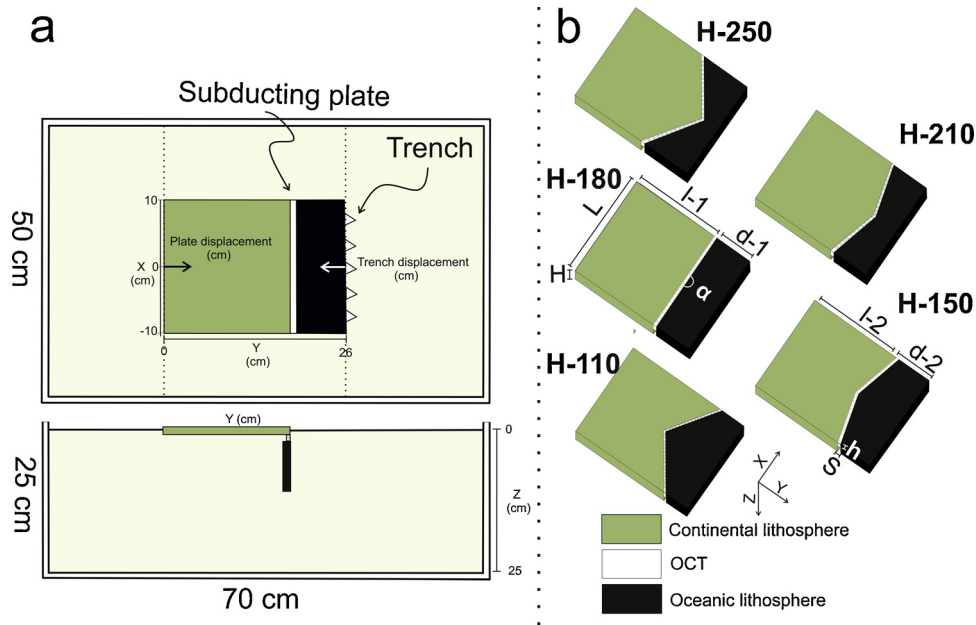


**Fig. 2.** a) Top view at subduction initiation and lateral view (at  $x = 0$  cm) after the OCT subduction. Dotted lines indicate the coordinate taken as a reference to measure either the plate displacement or the trench displacement. b) Geometries for the subducting lithosphere tested in this study (see Table 3).

**Table 3**  
Geometrical parameters of the models (see Fig. 2B).

Slab breakoff depths <sup>a</sup> (km)	Slab breakoff time <sup>b</sup> (Myr)	References	Key in Fig. 1
100-400	9-35	Gerya et al. (2004)	1
300	7	Regard et al. (2008)	2
405-510	2.5-6.7	Baumann et al. (2010)	3
280-400	9-21	Van Hunen and Allen (2011)	4
120-145	7-23	Duretz et al. (2014)	5
80-240	2-50	Freeburn et al. (2017)	6
200-300	23-35	Magni et al. (2017)	7
95-140	1.5-2.5	Schellart (2017)	8
240-260	16-32	Broerse et al. (2019)	9
290-310	12.5-27	Hertgen (2018)	10

<sup>a</sup> Range of depths at which the full break-off occurs.

<sup>b</sup> Time to the full breakoff since the arrival at the trench of the continental plate.

–80 kg/m<sup>3</sup>, respectively. In order to maintain the overall slab pull constant between models, the volume of the subducting oceanic lithosphere is identical in all the experiments irrespective of the geometry of the OCT. The length of the oceanic lithosphere therefore varies laterally as a function of the OCT orientation.

The passive margin, i.e. the transition from the continental to oceanic lithospheres (OCT), is considered as a weak zone of inherited deformation. This zone is 0.6 cm wide (equivalent to 45 km in Nature), 0.5 cm thick and is simulated with a less viscous layer of pure PDMS silicone (about one order of magnitude lower than the oceanic and continental lithospheres). The OCT silicone is homogeneously seeded with glass beads of 5 mm diameter at a 1 cm spacing, to represent rheological heterogeneities that could result from previous extensional events and to help localizing the deformation. This mixture exhibits a non-Newtonian behavior that can eventually lead to the rupture of the OCT. The combined density of the pure PDMS and seeds correspond to a positive density contrast of 180 kg/m<sup>3</sup>. The glucose syrup used to simulate the sub-lithospheric mantle has a Newtonian rheology. The slab to mantle viscosity ratio is  $\sim 1500$ , in the upper limits of values proposed in previous studies (Di Giuseppe et al., 2008; Funicello et al., 2008; Wu et al., 2008; Ribe, 2010; Di Caprio et al., 2011). The

assembled system (i.e the oceanic lithosphere, OCT and the continental lithosphere) is placed in the center of a 70 × 50 × 25 cm transparent plexiglass tank, filled with glucose syrup, in order to avoid potential lateral boundary effects (Fig. 2). Materials have been selected to simplify the temperature-dependent Earth rheological profile and to respect the standard procedure for stress scaled down for length, buoyancy, viscosity, in a natural gravity field ( $g_{\text{model}} = g_{\text{Nature}}$ ) as described by Weijermars and Schmeling (1986) and Davy and Cobbold (1991). From the simple scaling equations:

$$(t_{\text{nature}} / t_{\text{model}}) = ((\Delta\rho g)_{\text{model}} / (\Delta\rho g)_{\text{nature}}) \cdot (\eta_{\text{nature}} / \eta_{\text{model}}) \quad (1)$$

$$(U_{\text{nature}} / U_{\text{model}}) = (t_{\text{model}} L_{\text{nature}}) / (t_{\text{nature}} L_{\text{model}}) \quad (2)$$

where  $t$  is the time,  $\Delta\rho$  the density difference between the oceanic lithosphere and the asthenosphere,  $g$  the standard acceleration due to gravity,  $h$  the length,  $\eta$  the viscosity of the asthenosphere, and  $U$  the velocity, we find that 147 s and 1 cm in the experiment correspond to 1 Myr and 75 km in nature, respectively (Table 2).

## 2.2. Experimental procedure

We first perform a set of 5 experiments in which the initial geometry of the OCT is systematically changed (Fig. 2 and Table 3). In order to maintain the subduction symmetrical, the center of the subduction zone is taken as a symmetry axis (i.e.  $x = 0$ ). Therefore, models are either concave towards the trench (models H-110 and H-150), straight (model H-180) or convex towards the trench (models H-210 and H-250). A sixth experiment, with a geometry similar to model H-250, has been repeated to specifically track the topographic evolution.

We manually initiate subduction by forcing the leading edge of the oceanic silicone plate downwards into the glucose syrup. Each experiment is monitored during its entire duration by a sequence of digital pictures taken from the front and top views at a constant time interval of 30 s. The position of both sides of the weak zone was tracked on the frontal view. The slab is considered to be fully detached along a section when the leading edge of the continental lithosphere started moving back to the surface. The depth of slab break-off at a section is therefore the maximum depth reached by the continental lithosphere at that point. As the slab is vertical at the time of the slab breakoff, the length measured on the frontal view corresponds to the depth. On the top

view, we track the displacement in the trench-perpendicular direction (y-axis) of both the trench and the plate trailing edge at surface. As the evolution of the experiments is symmetrical around  $x = 0$  cm, the measurements (slab breakoff depth, timing and buoyancy forces) have been carried out along one side of the subduction zone. While the plate is initially 20 cm wide, its lateral deformation during subduction leads to a narrowing of the subduction zone, which limits the distance over which measurements can be done along trench.

We also track the topographic evolution of the model TH-250 with setup similar to the model H-250. To achieve this, we use a structure-from-motion technique that requires the surface to be tracked to have a texture. Therefore, we cover the model with a thin layer of light and coarse powders mixture (~0.1 cm thick). This layer increases the surface tension at the model surface, which in turn slows down the subduction velocity in the model. However, it does not affect the way the slab deforms, and the slab breakoff initiates and propagates.

### 3. Results

#### 3.1. Slab breakoff depth and timing

##### 3.1.1. Reference model (H-180)

The reference model (H-180) consists of a straight OCT parallel to the trench direction (Fig. 2 and Table 3), similar to what has been done in the previous studies. During the initial phase of oceanic subduction, slab pull leads to a trench retreat at velocities of ~0.6 cm/min. The arrival of the OCT at the trench occurs 5 min after the start of the experiment (Fig. 3), and after a few seconds, it is followed by the continental lithosphere (Figs. 3 and 4). Continental subduction results in a progressive decrease of both plate and trench velocities to values close to 0. The OCT is then progressively stretched owing to the combined effects of the negative buoyancy force of the oceanic slab segment and the positive buoyancy force of the continental slab segment. Once stretching is strong enough, the continental segment separates -i.e.

breakoff- from the oceanic segment (Fig. 4).

Slab breakoff occurs almost simultaneously in the central portion of the slab (between  $x = 0$  and  $x = 5.5$  cm, Fig. 2a) 34 min after the onset of continental subduction (Figs. 3 and 4), and then it laterally propagates towards the edges of the subduction zone. Once the oceanic lithosphere is completely detached, after 36 min, it continues to sink at a rate of 0.85 cm/min (~15.5 cm/yr in nature) while the continental subducted segment is educted towards the surface at an average rate of ~0.03 cm/min (0.55 cm/yr in nature).

In the reference model (Fig. 5), the continental lithosphere reaches a maximum depth of 3.3 cm (~250 km in nature) at the subduction zone center, 34 min (~14 Ma in nature) after the OCT arrival at the trench. Slab breakoff propagates laterally over the first 5 cm (375 km in nature) at the same depth of 3.3 cm. For the last 3 cm -i.e. at the slab edges- slab breakoff occurs at greater depths, with a peak at 3.7 cm (~280 km in nature). The lateral propagation of the breakoff is instantaneous for the first 5.5 cm, and its average velocity over the first 8 cm from the subduction zone center is ~4 cm/min (74 cm/yr in nature) (Fig. 5).

The main buoyancy forces involved in the system are that of the oceanic slab segment ( $F_{Bu-oc}$ ) and the continental slab segment ( $F_{Bu-co}$ ), which are expressed per meter length of trench as:

$$F_{Bu-oc} = \Delta\rho_{oc} g h_{oc} L_{oc} \quad (3)$$

$$F_{Bu-co} = \Delta\rho_{co} g h_{co} L_{co} \quad (4)$$

with  $\Delta\rho$  the density difference between the considered slab segment and the surrounding mantle,  $h$  the thickness of the slab and  $L$  the length of the considered slab segment. Note that the calculation of  $F_{Bu-co}$  includes both the continental segment and the OCT. The total buoyancy force writes as:

$$F_{Bu-tot} = F_{Bu-co} - F_{Bu-oc} \quad (5)$$

The buoyancy force related to the oceanic slab segment is computed from the measured length of the oceanic lithosphere at the time of slab breakoff for different sections along the subduction zone. The buoyancy

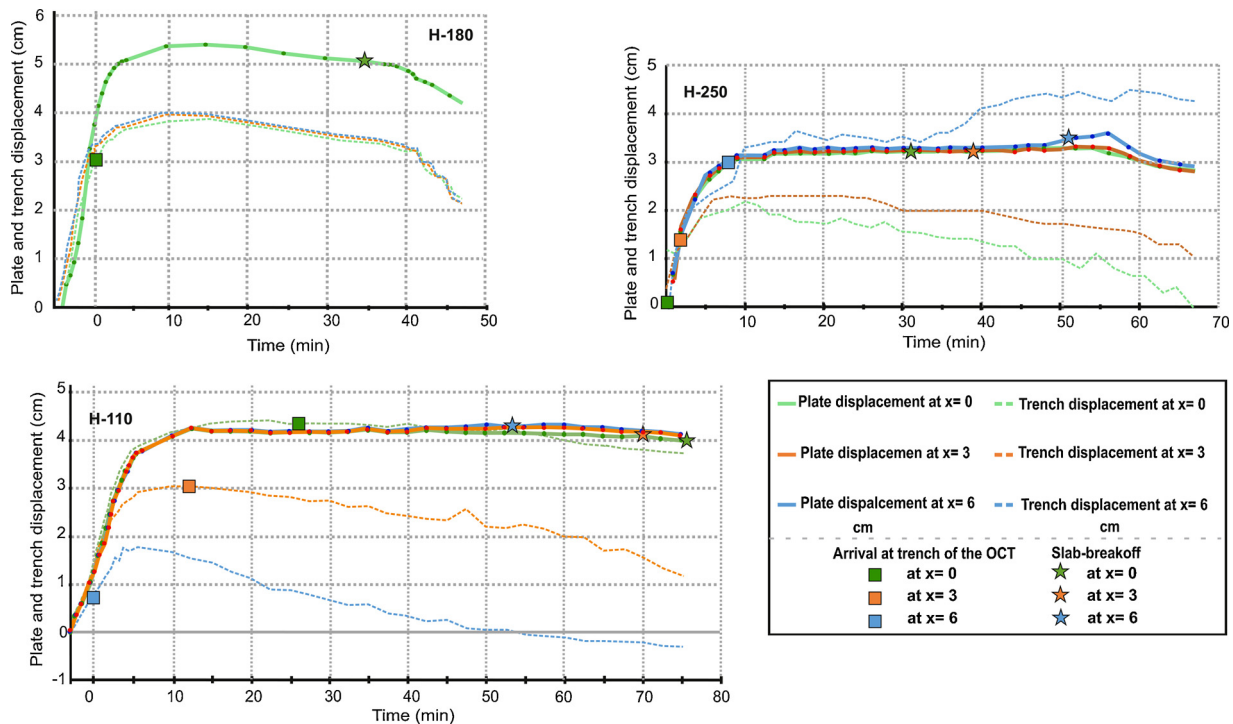
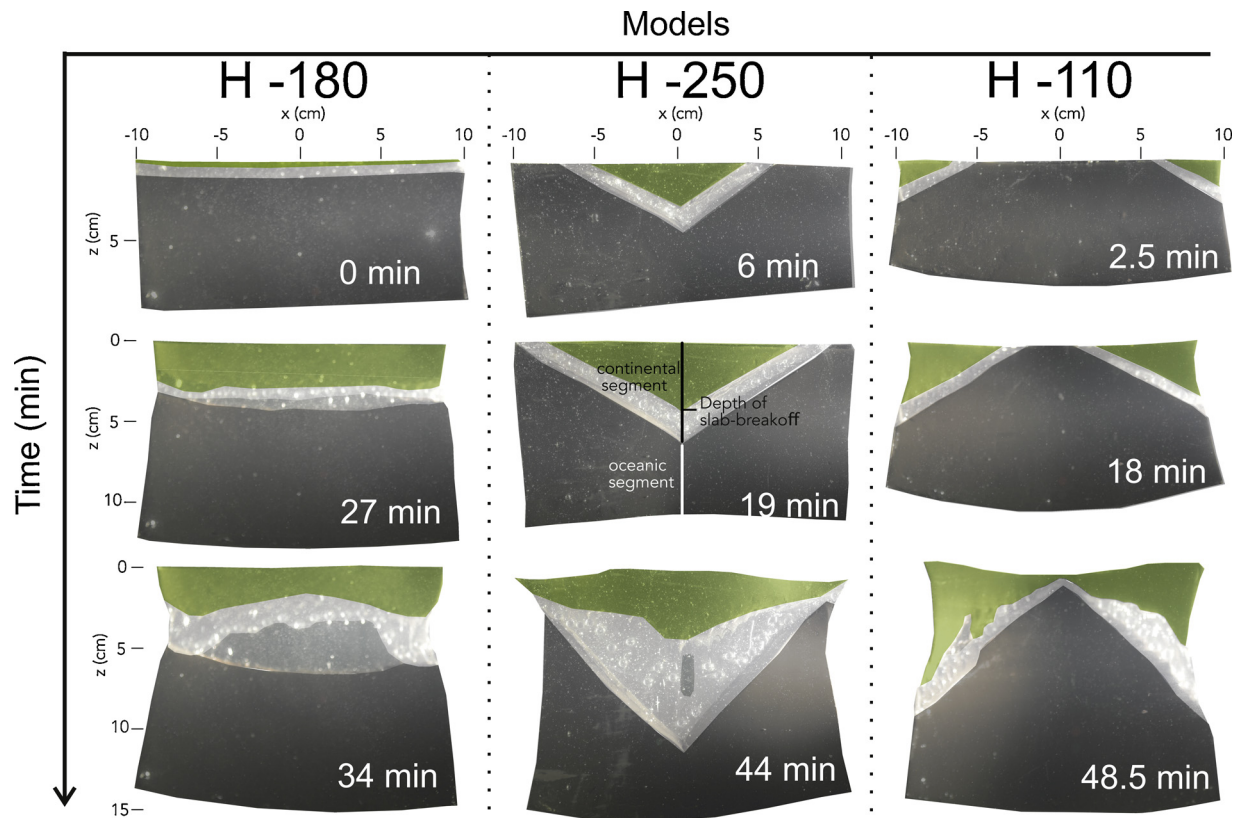


Fig. 3. Plate displacement (solid lines) and trench displacement (dotted lines) measured along three cross-sections perpendicular to the trench direction for models H-180, H-250 and H-110 (Fig. 2a). An increase in the plate displacement indicates that the plate is advancing towards the trench. An increase in the trench displacement indicates that the trench is advancing towards the subducting plate (rollback). The zero on the x-axis corresponds to the time of the arrival at the trench of the first piece of the continental lithosphere. Plate displacement for the model H-180 is identical along the three cross-sections.



**Fig. 4.** Frontal views of the reference model (H-180) and of the two end-member models (H-250 and H-110) at different stages of their evolution. The time indicated in each picture corresponds to the time after the arrival at the trench of the OCT. The first row shows the arrival at the trench of the OCT and of the continental lithosphere. The second-row corresponds to the phase of the OCT stretching for the model H-180 and to the progressive arrival at the trench of the OCT in the other models. The third row shows the lateral propagation of the slab breakoff.

force related to the continental slab segment is obtained by measuring the effective length of continental material driven into the mantle, which differs from the maximum depth of the continental leading edge (Fig. 5).  $F_{Bu-oc}$  is constant through the sections with a value of  $-0.66$  N/m (Fig. 6a). Continental buoyancy slightly decreases from the central section ( $0.43$  N/m) to the edges ( $0.28$  N/m), which gives a total force required to obtain the slab breakoff of  $1.09$  N/m in the center and  $0.94$  N/m at the edges (Fig. 6a).

### 3.1.2. Model H-250

The only difference between the model H-250 and the reference model H-180 is the OCT geometry, which instead of being straight ( $\alpha = 180^\circ$ ) is convex towards the trench ( $\alpha = 250^\circ$ ) (Fig. 2b and Table 3). It means that the initial angle between the trench and the OCT is  $35^\circ$  and that the continental subduction occurs first at the subduction zone center.

In the central section, the arrival of the OCT at the trench occurs 30 s after the onset of the experiment and it is followed, after a few seconds, by the continental lithosphere (Fig. 3). The OCT is then progressively subducted towards the edges of the subduction zone, and it arrives at the trench along the section located 6 cm away from the center of the subduction zone 7.5 min later (Figs. 3 and 4).

During the early stage of subduction, the oceanic lithosphere is consumed, and slab pull leads to an average slab roll back velocity of  $0.37$  cm/min (Fig. 5a). Because of the initial OCT geometry, the arrival of the continental lithosphere at the trench occurs first at the center of the subduction zone, while oceanic lithosphere is still being subducted laterally (Fig. 4). The OCT is stretched owing to the combined effects of buoyancy forces. Once stretching is large enough, the continental segment detaches from the oceanic segment (Fig. 4).

Slab breakoff first takes place along the central Section 31 min

( $\sim 13$  Ma in nature) after the onset of the continental lithosphere subduction (Fig. 3). It then propagates towards the sides of the subduction zone and occurs after 54 min ( $\sim 22$  Ma in nature) at 8 cm from the center (Fig. 5a).

The slab breakoff depth is different than in the reference model (Fig. 5b). Slab breakoff occurs at a depth of 4.6 cm (345 km in nature) at the central section and shallows to a minimum depth of 2.4 cm (180 km in nature) at  $x = 5$  cm. The rate of lateral propagation of the slab breakoff is almost constant ( $\sim 0.37$  cm/min, Fig. 5a).

Buoyancy forces at the time of slab breakoff also differ from the reference model (Fig. 6a). The buoyancy force of the oceanic slab segment changes from  $-0.32$  N/m to  $-0.70$  N/m, from the center to the edge of the subduction zone, respectively (Fig. 6b). The buoyancy force of the continental segment instead decreases from  $\sim 0.9$  N/m at the center to  $\sim 0.2$  N/m at  $x = 5$  cm (Fig. 6b), and then increases up to  $0.4$  N/m at the edge of the subduction zone. As a result, the total buoyancy force at slab breakoff are varying laterally in comparison to the reference model. From the center ( $x = 0$ ) to  $x = 5$  cm,  $F_{Bu-tot}$  decreases from  $1.20$  N/m to  $0.78$  N/m and increases to  $1.1$  N/m at  $x = 7$  cm.

### 3.1.3. Model H-110

In the model H-110 which is defined by  $\alpha = 110^\circ$  (Fig. 2b and Table 3), the OCT is concave towards the trench, with an initial trench-OCT angle of  $35^\circ$ . This implies that continental subduction first starts at the edges of the subduction zone (Fig. 4).

The OCT arrival at the trench occurs 3 min after the onset of the experiment (Fig. 3) and is followed by the subduction of the continental lithosphere at 4.5 min. Like in the model H-250, the OCT is then progressively subducted, and the trench arrives at the center after 26 min.

Slab breakoff occurs first at the slab edges ( $x = \sim 7$  cm) 54 min

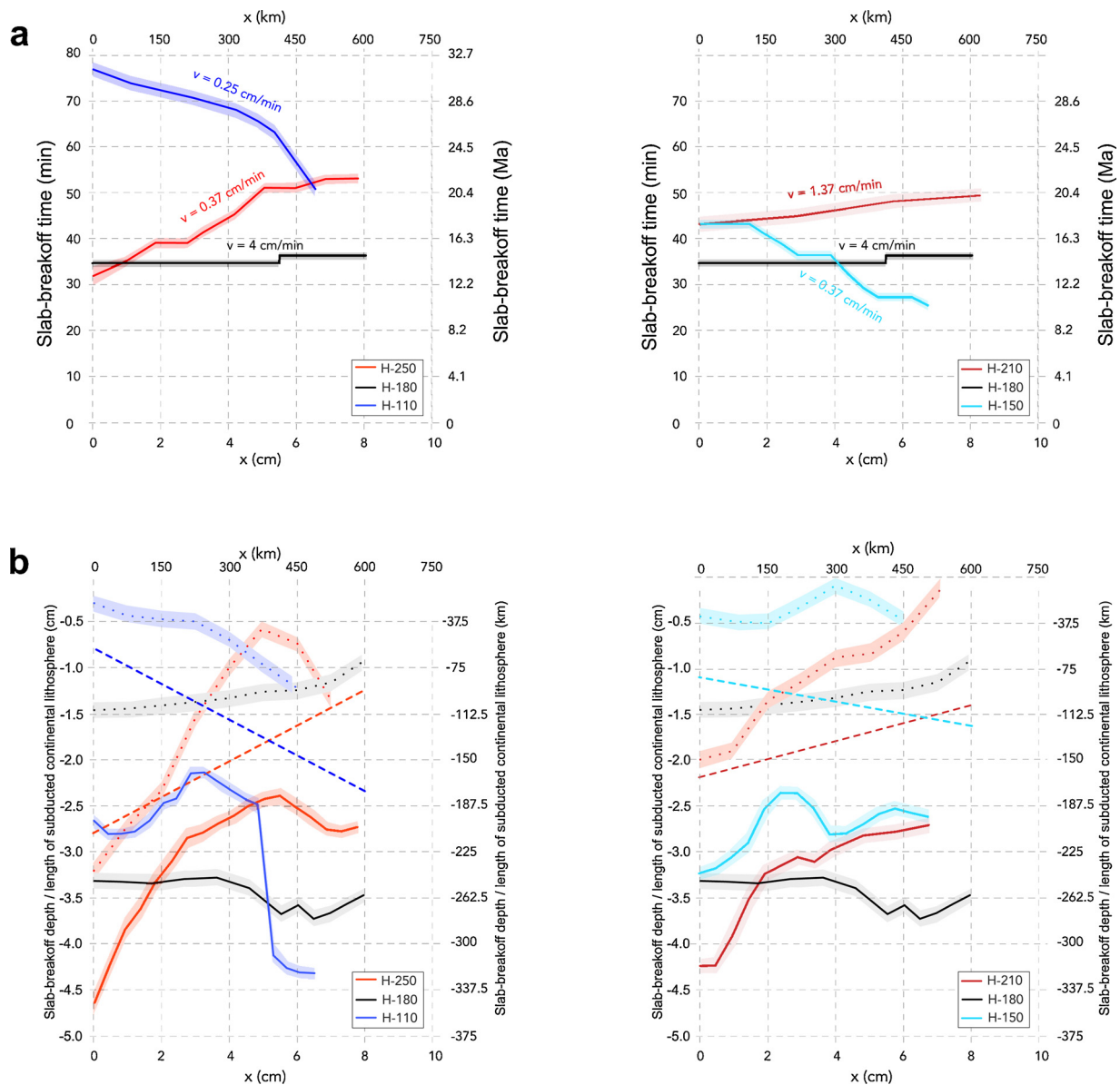


**Fig. 5.** a) Along-trench time for the slab to breakoff after the arrival of the continental lithosphere at the trench for the different models. Position  $x = 0$  cm corresponds to the center of the subduction zone (Fig. 2A). b) Depths of the slab breakoff along the subduction zone are indicated by solid lines. Observed lengths of the subducted continental lithosphere (dotted lines) are plotted against the predicted lengths of the subducted continental lithosphere (dashed lines), as obtained considering the buoyancy force required for the slab to breakoff in the central section of the reference model (1.1 N/m). Shaded colors indicate the measurements uncertainty.

after the OCT arrival at the trench (Fig. 5a), and then propagates toward the center of the subduction zone, where it ultimately develops at 76 min ( $\sim 31$  Ma in nature).

The concavity from the oceanic to the continental lithosphere determines the shape evolution of the subducting plate. The slab becomes narrower through time (Fig. 4). The slab breakoff depth is also highly variable (Fig. 5b), from 4.4 cm (330 km in nature) at the subduction zone edge to a minimum of 2.1 cm (160 km in nature) at  $x = 3$  cm. Slab breakoff laterally propagates at an almost constant velocity of  $\sim 0.25$  cm/min ( $\sim 5.5$  cm/yr in nature) (Fig. 5a).

Buoyancy forces change laterally (Fig. 6c). At the time of slab breakoff, the negative buoyancy force of the oceanic slab segment increases from the edge to the center of the subduction zone from  $\sim -0.5$  N/m to  $\sim -0.9$  N/m, respectively. The buoyancy force of the continental segment increases from  $\sim 0.1$  N/m at  $x = 0$  cm to  $\sim 0.37$  N/m at  $x = 6$  cm. The total buoyancy force also varies along the trench with the highest value of  $\sim 0.96$  N/m at the center of the

subduction zone and the lowest (0.90 N/m) at  $x = 3$  cm.

### 3.1.4. Models H-150 and H-210

Models H-150 and H-210 are intermediate models between the reference model and the two end-members described above (Fig. 2 and Table 3). They correspond to an initial angle of  $15^\circ$  between the OCT and the trench. They exhibit a range of slab breakoff depths that significantly differs from the reference model. For the model H-150, the slab breakoff occurs in between 2.4 cm at the subduction zone center and 3.3 cm at the subduction zone edge, while in the model H-210, it is between 2.7 cm at the subduction zone edge and 4.25 cm at the subduction zone center (Fig. 5b). Considering the time necessary for the slab breakoff to propagate along the entire subduction zone, these intermediate models are closer to the two end-members. It takes 19 min (in between 23 and 42 min) for the model H-150 and 7 min (in between 42 and 49 min) for the model H-210. Buoyancy forces acting on the OCT are between  $\sim 1$  N/m and  $\sim 0.75$  N/m for the model H-210 and

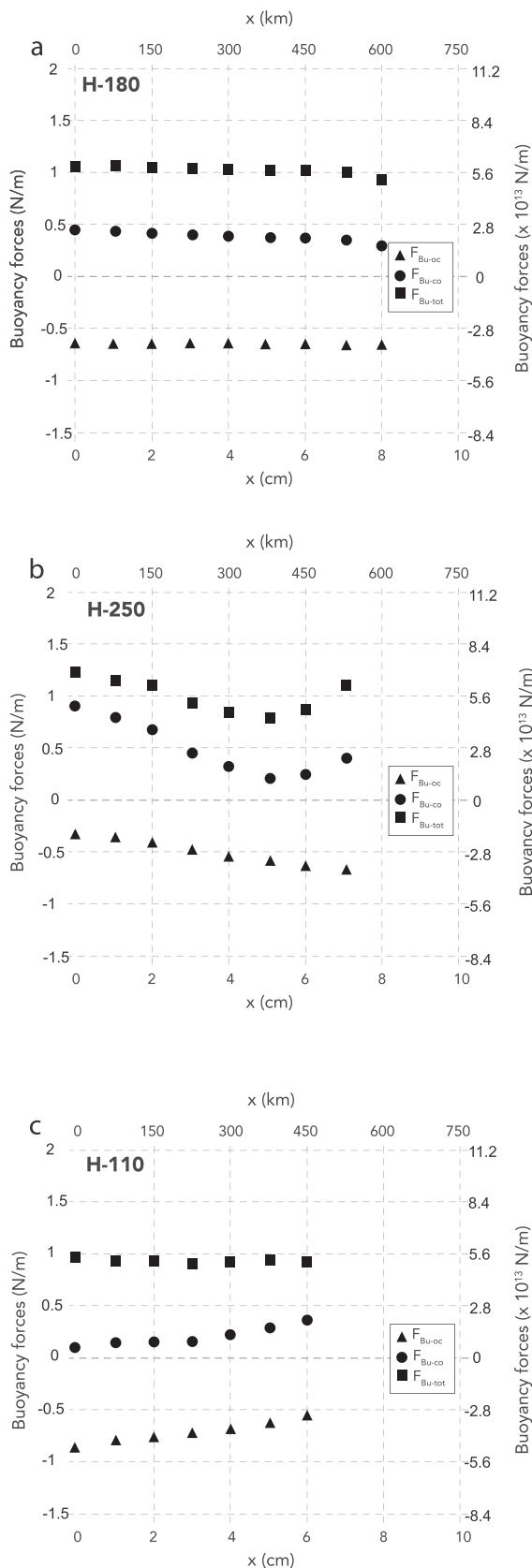


**Fig. 6.** Buoyancy forces acting on the slab at the time of the slab breakoff for models a) H-180, b) H-250 and c) H-110. x-axis represents the distance along the trench from the subduction zone center (see Figs. 2a). Triangles and circles correspond to the buoyancy force related to the oceanic ( $F_{Bu-oc}$ ) and continental ( $F_{Bu-co}$ ) slab segments, respectively. Squares correspond to the sum of both forces ( $F_{Bu-tot}$ ).

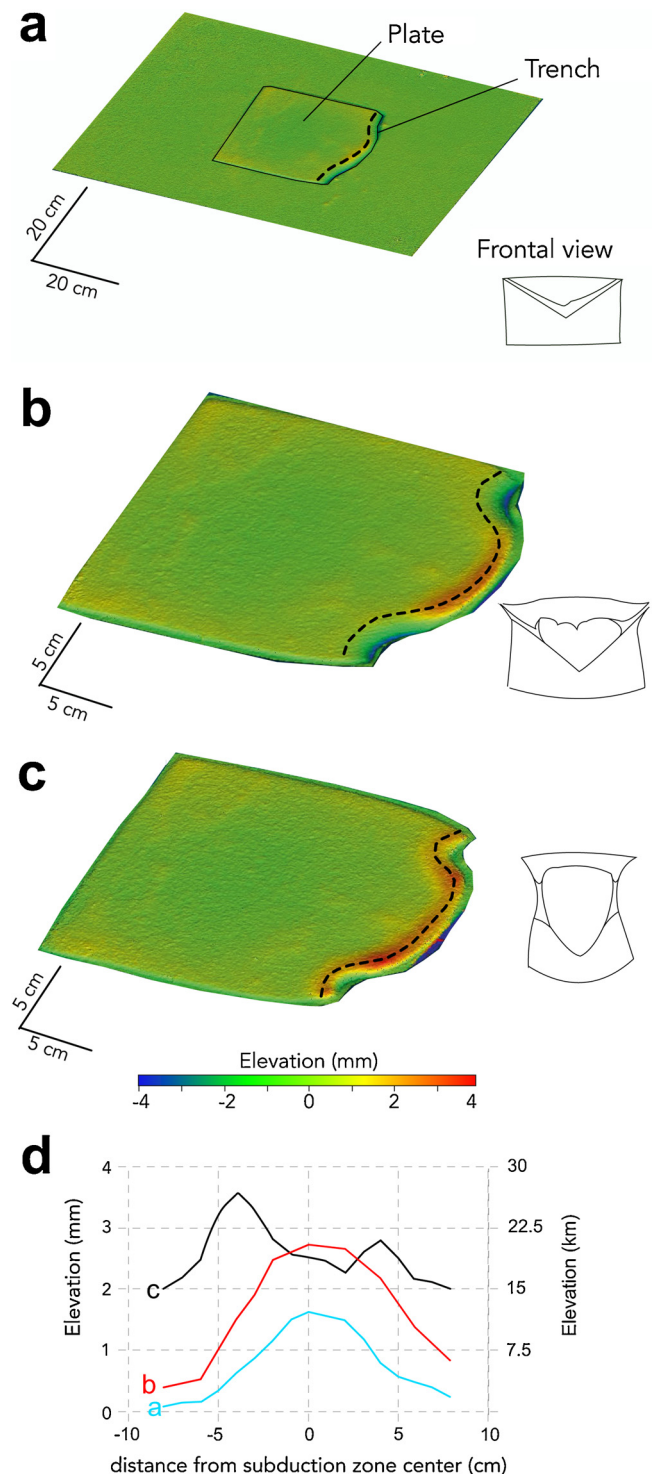


**Fig. 7.** Topography of the model TH-250. a) During the stretching of the OCT at the subduction zone center. b) During the lateral propagation of the slab breakoff. c) Once the breakoff is achieved along the entire length of the subduction zone. d) Profile of elevation measured along the dotted sections located 65 km away from the trench for stages A (blue), B (red) and C (black).

~0.92 N/m and ~ 0.76 N/m for the model H-150 (see Supplementary Material).

### 3.2. Surface topography

We tracked the vertical motions at the surface of the subducting plate resulting from the internal dynamics of our subduction system. In

Fig. 7, we show the topographic evolution of the model TH-250, whose initial configuration is similar to the model H-250. Fig. 7a shows the topography associated to the initiation of the slab breakoff at the subduction zone center (equivalent to 19 min in the model H-250). A zone of higher elevation (1.6 mm above the mean elevation of the plate) develops above the detaching slab in the center of the subduction zone while the subduction that is still active on both sides is associated with lower elevations. As the slab breakoff laterally propagates (Fig. 7b), the area at the surface affected by higher elevations also laterally propagates. A bulge with a trench-perpendicular extension of 10 mm shows a maximum elevation of 2.7 mm above the mean plate elevation. Between the two stages, the subduction zone center has uplifted by 1.1 mm. As the subduction is still active on the edges of the subduction zone, a deep trench is still present. Finally, the slab breakoff is fully achieved along the trench and the entire plate shows high elevations close to the trench (Fig. 7c). The zones of maximum elevation ( $\sim 3.5$  mm) correspond to the areas where the plate boundary is the most arcuate. The subduction zone center is downlifted by  $\sim 0.2$  mm during this stage.

## 4. Discussion

### 4.1. Slab breakoff dynamics

Our reference model (H-180) shows first-order similarities with previous 2D and 3D models of oceanic lithosphere subduction followed by continental lithosphere subduction (e.g., van Hunen and Allen, 2011; Pusok and Kaus, 2015; Menant et al., 2016; Magni et al., 2017). In particular, the depth and the timing of the breakoff following continental subduction in the model H-180 is within the range of previously obtained values in analogue and numerical models (Fig. 1) and those estimated for subduction zones on Earth (e.g., Mahéo et al., 2002; Chen et al., 2015), which indicates that the setup and the scaling adopted here are appropriate at first order to simulate the slab breakoff in subduction systems. Changing the rheological properties and/or dimensions of the OCT might impact the timing and the depth of the slab breakoff, but the precise quantification of their effect would require further studies.

We also observe that the slab breakoff initiates at the subduction zone center, in agreement with previous 3D models with a straight OCT (van Hunen and Allen, 2011; Duret et al., 2014). In our reference model, the total buoyancy force necessary to develop the slab breakoff is  $\sim 1.1$  N/m (equivalent to  $\sim 6.2 \times 10^{13}$  N/m in nature). The breakoff is delayed at the slab edges because the vertical stretching at this location results in the shortening of the slab in two horizontal directions ( $x$  and  $y$ ). Therefore, the necking only develops when the tensile stresses responsible for the vertical stretching are high enough. It could be achieved either by subducting more continental lithosphere or by decreasing the surface over which the slab pull is applied. Fig. 6 shows that the buoyancy force of the continental slab instead decreases toward the edge. Slab breakoff at the edges occurs after the breakoff at the center, which allows tensile stresses to increase at the edges by decreasing the surface over which the total buoyancy force is applied. Such increase in tensile stresses also results in an increased stretching of the continental lithosphere, which explains why the slab breakoff occurs at higher depths at the edges ( $\sim 280$  km instead of  $\sim 250$  km) despite a lesser amount of subducted continental lithosphere. In addition, the lateral propagation rate of the slab breakoff, which is on average equivalent to about  $\sim 75$  cm/yr in model H-180, is in the same range to that found for young and weak subducting oceanic lithospheres (van Hunen and Allen, 2011). The slab break-off occurs at depths shallower than  $\sim 265$  km in our model, while it develops at  $\sim 280$ – $400$ -km depths in van Hunen and Allen (2011). The difference in the breakoff depth may come from both the density contrast between the continental lithosphere and the surrounding mantle and from the approximation chosen to describe the lithosphere rheology.

Our other models show, for the first time, the influence of the paleogeography of the subducted passive margin (i.e. OCT) on the slab breakoff dynamics. Changing the angle between the trench and the ocean and continent transition zone impacts the kinematics and the dynamics of the slab breakoff. In particular, the range of slab breakoff depths varies, from  $\sim 2.1$  cm ( $\sim 160$  km in nature) in model H-110 to  $\sim 4.6$  cm ( $\sim 345$  km in nature) in model H-250 (Fig. 1). Model H-180 shows that the breakoff occurs in the center of the subduction zone when the continental segment reaches a depth of 3.3 cm (250 km in nature). In this model, the buoyancy force of the oceanic slab is constant along the subduction zone. In the other models, to keep the negative buoyancy force of the entire oceanic slab constant, we accordingly changed the length of the oceanic segment along the trench (from 4 to 11 cm in the models H-110 and H-250, and from 6 to 9 cm in the models H-150 and H-210). Given the density difference between the oceanic and continental segments, the length of the subducted continental lithosphere should be lower where the oceanic segment is longer as less continental material is needed to get sufficient total buoyancy forces to trigger breakoff. This is what is indeed observed (Fig. 5), but the variation in the length of the subducted continental lithosphere is not linear as could be expected from the initial imposed linear change in the geometry. The observed length of the subducted continental lithosphere departs from the theoretical value, computed by considering the total buoyancy force (1.1 N/m) reached at the centre of the reference model (H-180). In the model H-250 for instance, the length of the subducted continental lithosphere is lower than anticipated for  $x > 2$  cm. Predicted lengths of subducted continental lithosphere only consider the local buoyancy forces. However, once breakoff starts at the subduction zone center and propagates laterally, the OCT length decreases. In turn, the tensile stress that applies to the remaining slab segment increases. As a consequence, less continental material is needed to reach the required level of stress to initiate the break off. The minimum length of the subducted continental lithosphere is 6 mm, a value reached at  $x = 5$  cm.

Another consequence of this lateral variation is that the stretching of the continental lithosphere (difference between the slab breakoff depth and the length of subducted continental lithosphere) increases from the center of the subduction zone towards the edges with a maximum at  $x = 5$  cm. Finally, when the breakoff approaches the slab edge, shortening parallel to the trench direction also develops, which may require, in this case, increasing the local buoyancy forces by subducting additional continental material (Fig. 5). The slab breakoff depth also varies, but follows the trend of the length of the subducted continental lithosphere. The difference between both curves shows that the stretching of the continental lithosphere increases towards the subduction zone edge following the propagation of the breakoff, similar to what is found in the reference model. Buoyancy forces therefore not only result in the deformation of the OCT, but also in the laterally variable deformation of the subducted continental material. The same applies to the model H-110, except that the slab breakoff occurs first at the subduction edge. In this model the stretching of the continental lithosphere is maximum at  $x = 5$  cm (Fig. 5). In the models where the obliquity of the OCT is less pronounced, the length of the subducted continental material is lower than expected: 0.1–0.5 cm (7.5–37.5 km in nature) in the model H-150 and  $\sim 0.12$ – $2$  cm (9–150 km in nature) in the model H-210.

The timing of the slab breakoff and the propagation rate also vary among the models (Fig. 5). With a straight OCT, the slab breakoff occurs almost instantaneously in the first 5.5 cm along the trench and is fully achieved for the remaining 2.5 cm after 2 min. It gives an average propagation rate of  $\sim 4$  cm/min ( $\sim 74$  cm/yr). Whereas, changing the obliquity of the OCT increases the time necessary for a complete breakoff of the slab. It requires 21 min ( $\sim 8.6$  Ma in nature) and 26 min ( $\sim 10.6$  Ma in nature) after the continental subduction started for models H-250 and H-110, respectively. The corresponding average lateral propagation rate is one order of magnitude lower than that of

the reference model, which evidences the importance of the location of the slab breakoff initiation on its kinematics. Trench parallel shortening of the OCT, close to the slab edges, delays the breakoff time and therefore the models in which the breakoff starts at the slab edges may require a longer time to initiate. For the slab width tested here (equivalent to 1500 km in nature), we observe time delays of up to 26 min ( $\sim 10.6$  Ma in nature) between the initiation of the breakoff on one side of the subduction zone and the full breakoff along the entire subduction zone. Such lateral variations in the timing of the breakoff may leave an imprint in the geological record (time variations of the uplift pattern, the anomalous volcanism), and could be used to get insights into the subducted passive margin geometry.

#### 4.2. Topographic evolution

The topography of the subducting plate is also affected by the slab breakoff dynamics. We modeled the topographic evolution of the model TH-250, which has an initial configuration similar to the model H-250. The absolute scaled values obtained here are too high owing to the simplification of the chosen lithospheric rheology as well as the absence of surface processes. However, the temporal and spatial variations of the topographic pattern can give us insights into the processes occurring at depths (Fig. 7). Initially, the OCT arrives at the trench in the central section, while the oceanic material is still subducted elsewhere, and starts stretching under the tensile stresses (Fig. 7a). During this time, at a distance equivalent to 65 km from the trench, the plate topography is  $\sim 1.5$  mm higher than the mean elevation of the plate (Fig. 7d). We interpret the anomalous high elevation at the subduction zone center as a consequence of the isostatic adjustment that results from the loss of mechanical continuity between the oceanic and the continental slab segments. The slab breakoff then laterally propagates, increasing the tensile stresses on the edges (Fig. 7b). At the surface, it correlates with anomalously high topography (up to 2.8 mm) and corresponds to an uplift of 1–1.3 mm with respect to the previous stage (Fig. 7c). This uplift could result from the combination of i) an isostatic uplift in areas that lost the mechanical continuity and ii) a dynamic uplift resulting from both a mantle upwelling through the now-opened slab window in the center of the subduction zone (Guillaume et al., 2010) and a continental slab eduction. In Fig. 7c, the continental lithosphere is fully detached from the oceanic lithosphere along a width of  $\sim 10$  cm in the trench-parallel direction. Fig. 7c also shows that areas that were affected by the slab breakoff on the subduction zone sides exhibit a net uplift of 1–2 mm. Interestingly, two zones of high topography are visible at  $x = -4$  cm and  $x = 4$  cm with values of  $\sim 3.5$  mm and  $\sim 2.7$  mm, respectively. The mechanisms responsible for these topographic highs could be similar to the ones at play in the central section of the subduction zone during the previous stage. The analysis of the model H-250 shows that the amount of the subducted continental lithosphere decreases toward the edges of the subduction zone and

therefore, the isostatic contribution after the slab breakoff in this region is less important than in the center of the subduction zone. The subsidence observed in the central section in the final stage could be a result of the cessation of the mantle upwelling along with the isostatic readjustment related to the eduction of the continental segment in this domain. A precise quantification of the respective contributions of the two processes would require a precise analysis of the mantle flow and slab geometry in three dimensions, which is not achievable in our models.

#### 4.3. Importance of passive margins orientation to understand and predict slab breakoff in nature

Our models are simplified representations of the subduction system. In particular, we do not simulate the upper/lower mantle boundary with a viscosity jump, which prevents any slab flattening and support from the lower mantle. As a consequence, if subduction of the continental lithosphere occurs late in the subduction history, the lateral variation in the negative slab pull that we introduce in our models with a non-straight OCT may be less important. This may temper the observed variations in slab breakoff depth. However, the stress that applies on the still attached OCT may still increase once the breakoff has started, which should produce lateral variations in the slab breakoff timing and depth. Another limitation of our setup is the lack of an overriding plate. It may impact the kinematics of the system by decreasing the subduction and trench velocities (e.g., Yamato et al., 2009), which may increase the timing of slab breakoff initiation and possibly reduce the lateral propagation rate. As a consequence, the propagation rates proposed here may be seen as an upper bound. The slab breakoff depth, instead, only depends on the properties of the subducting plate and should not vary when an upper plate is added to the system.

Despite all these limitations, our models show first order-differences in the dynamics of the slab breakoff that depend on the geometry of the transition between oceanic and continental lithospheres. Such non-straight cases may occur in nature, as derived from reconstructions for the Western Mediterranean (e.g., Vergés and Fernández, 2012), the Aegean (e.g., Jolivet et al., 2013) and other regions, like the Banda Arc.

The Banda Arc shape has been proposed to be the consequence of the compression between the Australian plate and the SE Asia (Carter et al., 1976; Bowin et al., 1980), or the result of the interaction between two subducted slabs (Cardwell and Isacks, 1978; Mc Caffrey, 1989). Recent studies (Spakman and Hall, 2010; Pownall et al., 2013) propose new interpretations inferred from seismic tomography images and fieldwork. In the model proposed by Spakman and Hall (2010), the slab-rollback is one of the primary mechanisms to explain the curvature of the slab in this region. It started 15 Myr ago (Fig. 8a) and progressively consumed oceanic material towards the embayment of the South Banda Sea. Along the northern margin, slab-rollback led to the delamination of

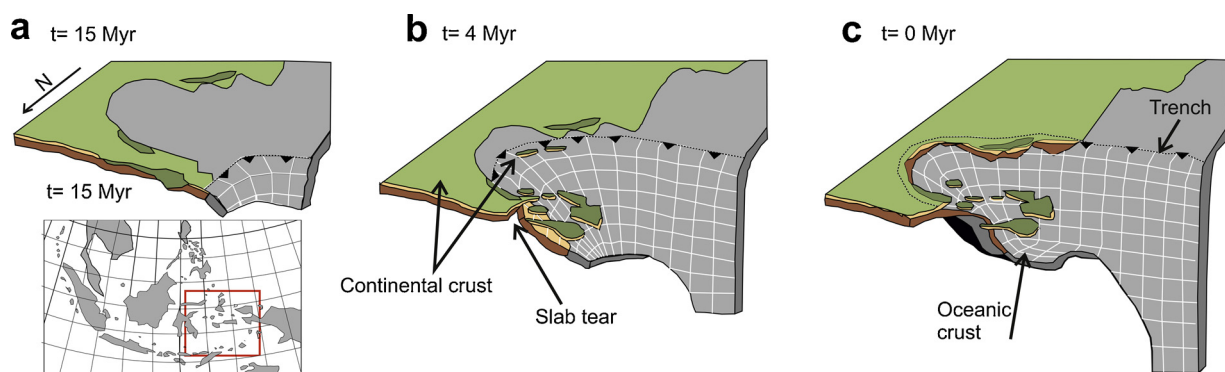


Fig. 8. Model of the evolution of the Banda Arc region over the last 15 Ma (modified from Spakman and Hall, 2010). a) Slab rollback onset. b) Tearing along the continental margin. c) Slab-flattening in the upper mantle and tearing propagation along the subducted continental margin.

the continental crust from the lithosphere in between 15 and 7 Ma (Fig. 8b). In their model, this part of the subducted slab incorporated delaminated continental lithosphere, leading to tearing and rotation of the slab and ultimately bringing it to its present-day position. Despite a difference in the width of the subduction zone, our model H-110 (Fig. 4) shares some geometrical similarities with the reconstruction proposed by Spakman and Hall (2010), with an obliquity between the oceanic to continental lithosphere transition and the trench. Continental material, at the edge of the subduction zone (equivalent to the northern margin of the Banda Arc region, Fig. 8a) arrived at the trench due to the slab-rollback. As a consequence, our model suggests that the arrival of continental material may also help initiating slab breakoff at this specific location. It also predicts that the slab breakoff should propagate towards the south, at shallower depths, as less continental material would need to be subducted. As shown in our models, the timing of propagation depends on the geometry and the length of the OCT. It may therefore require few million years before a complete breakoff of the slab beneath the Banda Arc is achieved.

## 5. Conclusions

We performed the first series of laboratory experiments investigating the dynamics of three-dimensional slab breakoff and its consequences at the surface for the topography and the subducting plate kinematics.

- The initial configuration of the subducting plate, and the orientation of the oceanic to continental lithosphere transition (OCT) in particular, controls the depth and the timing of slab breakoff. We showed that the slab breakoff occurs in a limited depth range when the OCT is parallel to the trench (250–280 km) whereas in models with a non-straight OCT, the slab breakoff depth significantly varies along the subduction zone by as much as ~170 km.
- The timing of the slab breakoff is also dependent on the initial geometry. In the model with an OCT parallel to the trench, the complete breakoff along the entire subduction zone is almost instantaneous at geological time scales (~2 Ma to propagate for 1200 km), whereas it is delayed for the non-straight OCT models, as oceanic subduction is temporarily maintained laterally. It can take up to ~9 Ma and ~12 Ma to obtain the breakoff at a same distance along the subduction, for models with an OCT convex towards the trench and concave towards the trench, respectively.
- The topographic evolution at the surface of the subducting plate reflects the evolution of the slab deformation at depths, and could be used to reconstruct the past history of the slab deformation in subduction systems. The exhumation of continental lithosphere, isostatic adjustment, and mantle upwelling all contribute at different levels to shape the plate's surface.

## Declaration of Competing Interest

The authors declare that they have no known competing financial interests or personal relationships that could have appeared to influence the work reported in this paper.

## Acknowledgments

This work has been supported by the European Research Council and the Horizon2020 Marie Curie ETN #674899 SUBITOP. The authors would like to thank J.J. Kermarrec for his invaluable technical assistance in the laboratory and Francesca Funicello and Fabio Corbi of the Laboratory of Experimental Tectonics (Università Roma Tre) for performing the rheological tests of the materials employed in this work through the EPOS Transnational Access. We also thank Joseph Martinod and an anonymous reviewer for their constructive comments, and Ajay Kumar for his careful text editing.

## Appendix A. Supplementary data

Supplementary material related to this article can be found, in the online version, at doi:<https://doi.org/10.1016/j.tecto.2019.228223>.

## References

- Baumann, C., Gerya, T.V., Connolly, J.A., 2010. Numerical Modelling of Spontaneous Slab Breakoff Dynamics During Continental Collision 332. Geological Society, London, Special Publications, pp. 99–114. <https://doi.org/10.1144/SP332.7>. 1.
- Bellahsen, N., Faccenna, C., Funicello, F., 2005. Dynamics of subduction and plate motion in laboratory experiments: insights into the “plate tectonics” behavior of the Earth. *J. Geophys. Res. Solid Earth* 110 (B1). <https://doi.org/10.1029/2004JB002999>.
- Boutelier, D., Cruden, A.R., 2017. Slab breakoff: insights from 3D thermo-mechanical analogue modelling experiments. *Tectonophysics* 694, 197–213. <https://doi.org/10.1016/j.tecto.2016.10.020>.
- Bowin, C., Purdy, G.M., Johnston, C., Shor, G., Lawver, L., Hartono, H.M.S., Jezek, P., 1980. Arc-continent collision in Banda Sea region. *AAPG Bull.* 64 (6), 868–915. <https://doi.org/10.1306/2f9193cd-16ce-11d7-8645000102c1865d>.
- Broerse, T., Norder, B., Govers, R., Sokoutis, D., Willingshofer, E., Picken, S.J., 2019. New analogue materials for nonlinear lithosphere rheology, with an application to slab break-off. *Tectonophysics* 756, 73–96. <https://doi.org/10.1016/j.tecto.2018.12.007>.
- Brun, J.P., Faccenna, C., 2008. Exhumation of high-pressure rocks driven by slab rollback. *Earth Planet. Sci. Lett.* 272 (1–2), 1–7. <https://doi.org/10.1016/j.epsl.2008.02.038>.
- Cardwell, R.K., Isacks, B.L., 1978. Geometry of the subducted lithosphere beneath the Banda Sea in eastern Indonesia from seismicity and fault plane solutions. *J. Geophys. Res. Solid Earth* 83 (B6), 2825–2838. <https://doi.org/10.1029/JB083iB06p02825>.
- Carter, D.J., Audley-Charles, M.G., Barber, A.J., 1976. Stratigraphical analysis of island arc—continental margin collision in eastern Indonesia. *J. Geol. Soc.* 132 (2), 179–198. <https://doi.org/10.1144/gsjgs.132.2.0179>.
- Chen, L., Qin, K.Z., Li, G.M., Li, J.X., Xiao, B., Zhao, J.X., Fan, X., 2015. Zircon U–Pb ages, geochemistry, and Sr–Nd–Pb–Hf isotopes of the Nuri intrusive rocks in the Gangdese area, southern Tibet: constraints on timing, petrogenesis, and tectonic transformation. *Lithos* 212, 379–396. <https://doi.org/10.1016/j.lithos.2014.11.014>.
- Davies, J.H., von Blanckenburg, F., 1995. Slab breakoff: a model of lithosphere detachment and its test in the magmatism and deformation of collisional orogens. *Earth Planet. Sci. Lett.* 129 (1–4), 85–102. [https://doi.org/10.1016/0012-821X\(94\)00237-S](https://doi.org/10.1016/0012-821X(94)00237-S).
- Davy, P., Cobbold, P.R., 1991. Experiments on shortening of a 4-layer model of the continental lithosphere. *Tectonophysics* 188 (1–2), 1–25. [https://doi.org/10.1016/0040-1951\(91\)90311-F](https://doi.org/10.1016/0040-1951(91)90311-F).
- Di Caprio, L., Gurnis, M., Müller, R.D., Tan, E., 2011. Mantle dynamics of continentwide Cenozoic subsidence and tilting of Australia. *Lithosphere* 3 (5), 311–316. <https://doi.org/10.1130/L140.1>.
- Di Giuseppe, E., Van Hunen, J., Funicello, F., Faccenna, C., Giardini, D., 2008. Slab stiffness control of trench motion: insights from numerical models. *Geochim. Geophys. Res.* 13 (2). <https://doi.org/10.1029/2007GC001776>.
- Duret, T., Gerya, T.V., Spakman, W., 2014. Slab detachment in laterally varying subduction zones: 3-D numerical modeling. *Geophys. Res. Lett.* 41 (6), 1951–1956. <https://doi.org/10.1002/2014GL059472>.
- Forsyth, D., Uyeda, S., 1975. On the relative importance of the driving forces of plate motion. *Geophys. J. Int.* 43 (1), 163–200. <https://doi.org/10.1111/j.1365-246X.1975.tb00631.x>.
- Freeburn, R., Bouilhol, P., Maunder, B., Magni, V., Van Hunen, J., 2017. Numerical models of the magmatic processes induced by slab breakoff. *Earth Planet. Sci. Lett.* 478, 203–213. <https://doi.org/10.1016/j.epsl.2017.09.008>.
- Funicello, F., Faccenna, C., Giardini, D., Regenauer-Lieb, K., 2003. Dynamics of retreating slabs: 2. Insights from three-dimensional laboratory experiments. *J. Geophys. Res. Solid Earth* 108 (B4). <https://doi.org/10.1029/2001JB000896>.
- Funicello, F., Faccenna, C., Heuret, A., Lallemand, S., Di Giuseppe, E., Becker, T.W., 2008. Trench migration, net rotation and slab–mantle coupling. *Earth Planet. Sci. Lett.* 271 (1–4), 233–240. <https://doi.org/10.1016/j.epsl.2008.04.006>.
- Gerya, T.V., Yuen, D.A., Maresch, W.V., 2004. Thermomechanical modelling of slab detachment. *Earth Planet. Sci. Lett.* 226 (1–2), 101–116. <https://doi.org/10.1016/j.epsl.2004.07.022>.
- Goes, S., Agrusta, R., Van Hunen, J., Garel, F., 2017. Subduction-transition zone interaction: a review. *Geosphere* 13 (3), 644–664. <https://doi.org/10.1130/GES01476.1>.
- Guillaume, B., Moroni, M., Funicello, F., Martinod, J., Faccenna, C., 2010. Mantle flow and dynamic topography associated with slab window opening: insights from laboratory models. *Tectonophysics* 496 (1–4), 83–98. <https://doi.org/10.1016/j.tecto.2010.10.014>.
- Hertgen, S., 2018. Comportement mécanique des roches et dynamique des lithosphères dans les zones de convergence. PhD thesis 1 Université de Rennes 284 p.
- Hippolyte, J.C., Angelier, J., Roure, F.B., 1994. A major geodynamic change revealed by Quaternary stress patterns in the Southern Apennines (Italy). *Tectonophysics* 230 (3–4), 199–210. [https://doi.org/10.1016/0040-1951\(94\)90135-X](https://doi.org/10.1016/0040-1951(94)90135-X).
- Husson, L., Guillaume, B., Funicello, F., Faccenna, C., Royden, L.H., 2012. Unraveling topography around subduction zones from laboratory models. *Tectonophysics* 526, 5–15. <https://doi.org/10.1016/j.tecto.2011.09.001>.
- Jolivet, L., Faccenna, C., Huet, B., Labrousse, L., Le Pourhiet, L., Lacombe, O., et al., 2013. Aegean tectonics: strain localisation, slab tearing and trench retreat. *Tectonophysics* 597, 1–33. <https://doi.org/10.1016/j.tecto.2012.06.011>.
- Magni, V., Allen, M.B., van Hunen, J., Bouilhol, P., 2017. Continental underplating after

- slab break-off. *Earth Planet. Sci. Lett.* 474, 59–67. <https://doi.org/10.1016/j.epsl.2017.06.017>.
- Mahéo, G., Guillot, S., Blichert-Toft, J., Rolland, Y., Pêcher, A., 2002. A slab breakoff model for the Neogene thermal evolution of South Karakorum and South Tibet. *Earth Planet. Sci. Lett.* 195 (1-2), 45–58. [https://doi.org/10.1016/S0012-821X\(01\)00578-7](https://doi.org/10.1016/S0012-821X(01)00578-7).
- Martinod, J., Funicello, F., Faccenna, C., Labanieh, S., Regard, V., 2005. Dynamical effects of subducting ridges: insights from 3-D laboratory models. *Geophys. J. Int.* 163 (3), 1137–1150. <https://doi.org/10.1111/j.1365-246X.2005.02797.x>.
- Mc Caffrey, Robert, 1989. Seismological constraints and speculations on Banda Arc tectonics. *Netherlands J. Sea Res.* 24 (2-3), 141–152. [https://doi.org/10.1016/0077-7579\(89\)90145-2](https://doi.org/10.1016/0077-7579(89)90145-2).
- Menant, A., Sternai, P., Jolivet, L., Guillou-Frottier, L., Gerya, T., 2016. 3D numerical modeling of mantle flow, crustal dynamics and magma genesis associated with slab roll-back and tearing: the eastern Mediterranean case. *Earth Planet. Sci. Lett.* 442, 93–107. <https://doi.org/10.1016/j.epsl.2016.03.002>.
- Pownall, J.M., Hall, R., Watkinson, I.M., 2013. Extreme extension across Seram and Ambon, eastern Indonesia: evidence for Banda slab rollback. *Solid Earth* 4 (2), 277–314. <https://doi.org/10.5194/se-4-277-2013>.
- Pusok, A.E., Kaus, B.J., 2015. Development of topography in 3-D continental-collision models. *Geochem. Geophys. Geosystems* 16 (5), 1378–1400. <https://doi.org/10.1002/2015GC005732>.
- Regard, V., Faccenna, C., Bellier, O., Martinod, J., 2008. Laboratory experiments of slab break-off and slab dip reversal: insight into the Alpine Oligocene reorganization. *Terra Nova* 20 (4), 267–273. <https://doi.org/10.1111/j.1365-3121.2008.00815.x>.
- Ribe, N.M., 2010. Bending mechanics and mode selection in free subduction: a thin-sheet analysis. *Geophys. J. Int.* 180 (2), 559–576. <https://doi.org/10.1111/j.1365-246X.2009.04460.x>.
- Rosenbaum, G., Lister, G.S., Duboz, C., 2002. Relative motions of Africa, Iberia and Europe during Alpine orogeny. *Tectonophysics* 359 (1-2), 117–129. [https://doi.org/10.1016/S0040-1951\(02\)00442-0](https://doi.org/10.1016/S0040-1951(02)00442-0).
- Royden, L.H., 1993. The tectonic expression slab pull at continental convergent boundaries. *Tectonics* 12 (2), 303–325. <https://doi.org/10.1029/92TC02248>.
- Schellart, W.P., 2005. Influence of the subducting plate velocity on the geometry of the slab and migration of the subduction hinge. *Earth Planet. Sci. Lett.* 231 (3-4), 197–219. <https://doi.org/10.1016/j.epsl.2004.12.019>.
- Schellart, W.P., 2017. A geodynamic model of subduction evolution and slab detachment to explain Australian plate acceleration and deceleration during the latest Cretaceous–early Cenozoic. *Lithosphere* 9 (6), 976–986. <https://doi.org/10.1130/L675.1>.
- Spakman, W., Hall, R., 2010. Surface deformation and slab–mantle interaction during Banda arc subduction rollback. *Nat. Geosci.* 3 (8), 562. <https://doi.org/10.1038/ngeo917>.
- Ton, S.W.A., Wortel, M.J.R., 1997. Slab detachment in continental collision zones: an analysis of controlling parameters. *Geophys. Res. Lett.* 24 (16), 2095–2098. <https://doi.org/10.1029/97GL01939>.
- van Hunen, J., Allen, M.B., 2011. Continental collision and slab break-off: a comparison of 3-D numerical models with observations. *Earth Planet. Sci. Lett.* 302 (1-2), 27–37. <https://doi.org/10.1016/j.epsl.2010.11.035>.
- Vergés, J., Fernández, M., 2012. Tethys–Atlantic interaction along the Iberia–Africa plate boundary: the Betic–Rif orogenic system. *Tectonophysics* 579, 144–172. <https://doi.org/10.1016/j.tecto.2012.08.032>.
- Weijermars, R., Schmeling, H., 1986. Scaling of Newtonian and non-Newtonian fluid dynamics without inertia for quantitative modelling of rock flow due to gravity (including the concept of rheological similarity). *Phys. Earth Planet. Inter.* 43 (4), 316–330. [https://doi.org/10.1016/0031-9201\(86\)90021-X](https://doi.org/10.1016/0031-9201(86)90021-X).
- Westaway, R., 1993. Quaternary uplift of southern Italy. *J. Geophys. Res. Solid Earth* 98 (B12), 21741–21772. <https://doi.org/10.1029/93JB01566>.
- Wu, B., Conrad, C.P., Heuret, A., Lithgow-Bertelloni, C., Lallemand, S., 2008. Reconciling strong slab pull and weak plate bending: the plate motion constraint on the strength of mantle slabs. *Earth Planet. Sci. Lett.* 272 (1-2), 412–421. <https://doi.org/10.1016/j.epsl.2008.05.009>.
- Yamato, P., Husson, L., Braun, J., Loiselet, C., Thieulot, C., 2009. Influence of surrounding plates on 3D subduction dynamics. *Geophys. Res. Lett.* 36 (7). <https://doi.org/10.1029/2008GL036942>.